ATMOSPHERIC MOISTURE TRANSPORT ACROSS THE SOUTHERN OCEAN

R.L. Slonaker
UCAR Visiting Scientist Program
NOAA/NESDIS, Office of Research and Applications, Camp Springs, MD, USA

M.L. Van Woert
NOAA/NESDIS, Office of Research and Applications, Camp Springs, MD, USA

1. INTRODUCTION

The Antarctic ice sheets are potentially a major source of water for the current rise in sea level, quantified as 1.8 mm yr^{-1} (*Douglas* 1991). The disintegration or regeneration of the West Antarctic ice sheet has implications for global sea level and global climate. A major constituent of the Antarctic ice sheet mass balance is the integrated accumulation rate.

Direct measurement of Antarctic precipitation is difficult. Coastline gauge collection is affected by the omnipresent winds and is frequently contaminated by blowing surface snow. Precipitation rates from the Antarctic interior are often below minimum gauge resolution (*Bromwich et al.* 1995). Glaciological precipitation measurements are accurate (*Lorius* 1983), but their spatial resolution is insufficient for integrated precipitation estimates of the entire continent.

Despite the significance of Antarctica and the surrounding Southern Ocean, there is a dearth of in situ measurements. TOVS and SSM/I observations are available twice daily at midlatitudes from each of two satellites, more so at higher latitudes due to orbital coverage overlap. Given the lack of traditional in situ measurements, it is logical to employ these remotely sensed data for determining atmospheric moisture transport across the Southern Ocean.

2. METHODOLOGY

2.1 Moisture flux calculation

Moisture flux calculation requires knowledge of the wind speed and direction in addition to the distribution of water vapor. The horizontal moisture flux vector is defined as

$$\mathbf{Q}(\lambda,\phi,t) = \int_{0}^{P_{surface}} \mathbf{V}(\lambda,\phi,p,t)\, q(\lambda,\phi,p,t)\, (g^{-1}\, dp) \qquad (1)$$

where **Q** represents the vertically integrated water vapor flux vector, λ is longitude, ϕ is latitude, t is time, p is the pressure level, **V** is the horizontal wind vector, q is the specific humidity, and g is the gravitational acceleration.

The pressure differential in (1) may be changed to a precipitable water differential provided the limits of integration are changed accordingly. The upper limit becomes $W_{surface}$, the surface value for precipitable water

$$\mathbf{Q}(\lambda,\phi,t) = \int_{0}^{W_{surface}} \mathbf{V}(\lambda,\phi,p,t)\, dW(\lambda,\phi,p,t) \qquad (2)$$

By integrating (2) along a boundary and through time, the atmospheric moisture transport can be determined.

V and dW are known at discrete pressure levels and layers respectively. The vertically integrated water vapor flux must be determined as a function of winds at these discrete levels and the differential water vapor for the intervening layers. By approximating the actual function with a piecewise linear function, the integration is performed via the trapezoidal rule (*Kreyszig* 1962)

$$\mathbf{Q}(\lambda,\phi,t) \equiv \sum_{i=1}^{n-1} \{0.5\, [\mathbf{V}_i(\lambda,\phi,t) + \mathbf{V}_{i+1}(\lambda,\phi,t)]\}\, dW_i(\lambda,\phi,t) \qquad (3)$$

where i is the integration step index (atmospheric layer index), and n-1 is the number of integration steps (number of atmospheric layers). As given in (3), the vertically integrated water vapor flux vector can be determined from available measurements.

2.2 Moisture and wind fields

Water vapor and virtual temperature fields were retrieved at NASA-GSFC as a part of the TOVS Path A product (*Susskind and Pfaendtner* 1989, *Susskind et al.* 1997). Due to inherent reduced informational content of infrared radiances, all observations with cloud fractions beyond 80% were deemed cloud-contaminated and reported as missing (*Susskind et al.* 1997). These regions required interpolation from surrounding areas where good quality data exist.

Over the oceans, changes in microwave surface emissivity as measured by certain SSM/I channels are correlated with the surface roughness and, hence, wind speed. The SSM/I is capable of obtaining ocean surface wind speeds to an accuracy of ± 2 m s^{-1} within the range of 3-25 m s^{-1}

(*Atlas et al.* 1996, *Hollinger et al.* 1987, *Goodberlet et al.* 1990). *Atlas et al.* (1993) used ECMWF analyses and conventional surface observations in a variational analysis to assign directions to the SSM/I wind speeds. *Slonaker and Van Woert* (1999) have noticed an anomaly in the surface wind speed distribution with very few values above 21 m s^{-1} for these data.

By combining the hypsometric and geostrophic equations, the thermal wind equation may be obtained which relates the vertical shear of geostrophic wind with the horizontal temperature gradient. Throughout middle and high latitudes, the large-scale wind field tends to be quasi-geostrophic with direction aligned with isobars and speed within roughly 15% of the geostrophic value (*Wallace and Hobbs* 1977). Using three-dimensional thermal data from the TOVS sounder, the thermal wind is computed from the following

$$Vg_1 - Vg_2 = (R_d/f) \ln (p_1/p_2) (\partial T_v/\partial n) \quad \textbf{(4)}$$

where f is the Coriolis parameter, R_d represents the dry air gas constant, p_1 and p_2 are the pressures of their respective levels, Vg_1 and Vg_2 represent the geostrophic wind speeds at corresponding levels, T_v is the mean virtual temperature of the intervening layer, and n is the horizontal unit vector perpendicular to the thermal wind.

The thermal wind provides a difference in geostrophic wind speed between two levels as a function of the horizontal gradient of mean virtual temperature of the intervening layer. If the wind field is known at some reference level in the vertical, then the thermal wind equation can be used to determine geostrophic winds throughout the column. The SSM/I-derived surface wind field (including both geostrophic and ageostrophic components) was then used in conjunction with thermal wind data to produce geostrophic wind fields at five upper-levels.

Water vapor and wind fields were thus known in three space dimensions and time from TOVS and SSM/I observations of the surface and atmospheric column. Horizontal winds were determined at the surface, 850 hPa, 700 hPa, 500 hPa, 300 hPa, and 100 hPa. Differential water vapor was known for the intervening layers. This information allowed the vertically integrated water vapor flux to be determined via (3).

3. VALIDATION

Radiosonde data were used to assess the overall quality of the satellite-derived data products and the moisture flux methodology. Here we compared radiosonde data from Macquarie Island to the

closest available satellite solution point. Figure 1 shows time series comparisons of vertically integrated meridional moisture transport for September 1988.

Table 1 shows comparison statistics generated from the Macquarie Island radiosonde data and satellite data for the one-year duration of this study in 1988. Table 1 shows the mean and standard deviation for comparable radiosonde and satellite data of meridional moisture flux estimates. The correlation coefficient between these two estimates is 0.84. Table 1 also presents difference statistics between radiosonde and satellite data. The higher standard deviation of the radiosonde data is expected considering the radiosonde is a point measurement while the satellite estimate represents conditions over a much larger spatial extent (2° latitude and 2.5° longitude).

Table 1. Statistical comparison of moisture flux estimates from Macquarie Island radiosonde (54.5°S, 158.9°E) and closest satellite solution (54.0°S, 158.8°E) for a one-year period during 1988. Only half of the available satellite data at this location were used in order to match the reporting interval of available radiosonde data. Spatial and temporal separations of these two data sources were approximately 56 km and 2 hours respectively.

	Meridional Moisture Flux ($kg\ m^{-1}\ s^{-1}$)	
Data Source	Mean	Standard Deviation
Macquarie Island Radiosonde	-41.6	129.8
Closest Satellite Solution	-47.9	105.9
Difference (Satellite minus Radiosonde)	-6.3	69.7

While encouraging, this comparison must be tempered by the fact that the satellite result and radiosonde data were not entirely independent. The direction of SSMI-derived surface wind vectors was determined predominately with ECMWF analyses (*Atlas et al.* 1996). The ECMWF analysis, however, incorporated all available radiosonde data. Therefore, the satellite-derived surface wind vectors depended to some extent on the radiosonde data at Macquarie Island.

Moreover, TOVS Path A layer-mean values of virtual temperature and precipitable water were created using a 6-hour forecast as initialization. The forecast was generated from an analysis, which was based on all available data sources, including radiosondes. Thermal wind and moisture data of the satellite solution were dependent on Macquarie Island radiosonde data collected 6-18 hours prior to the satellite observations. They were, however, independent of simultaneous radiosonde data.

Figure 1. Time series of vertically integrated meridional moisture transport estimates (kg m^{-1} s^{-1}) from satellite and radiosonde data sources at Macquarie Island during September 1988.

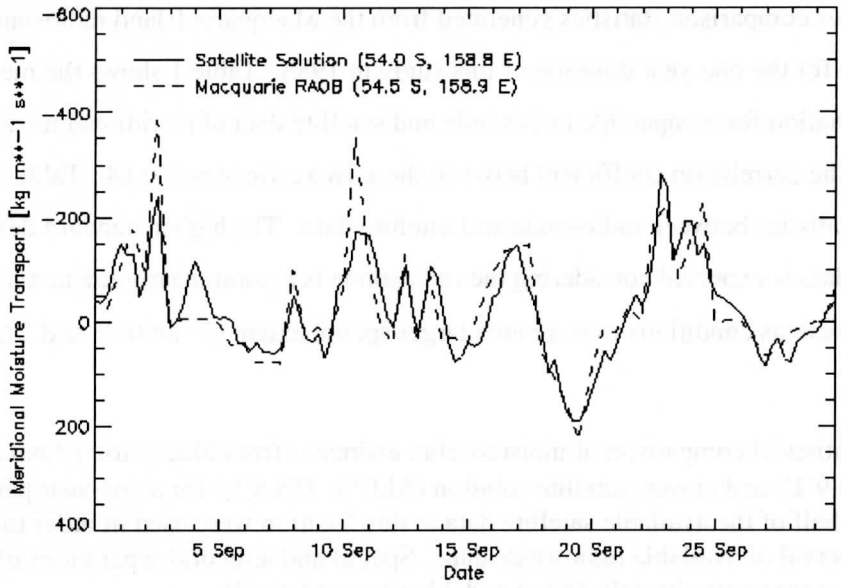

Figure 2. Southern Ocean latitude boundaries used for meridional moisture transport analyses.

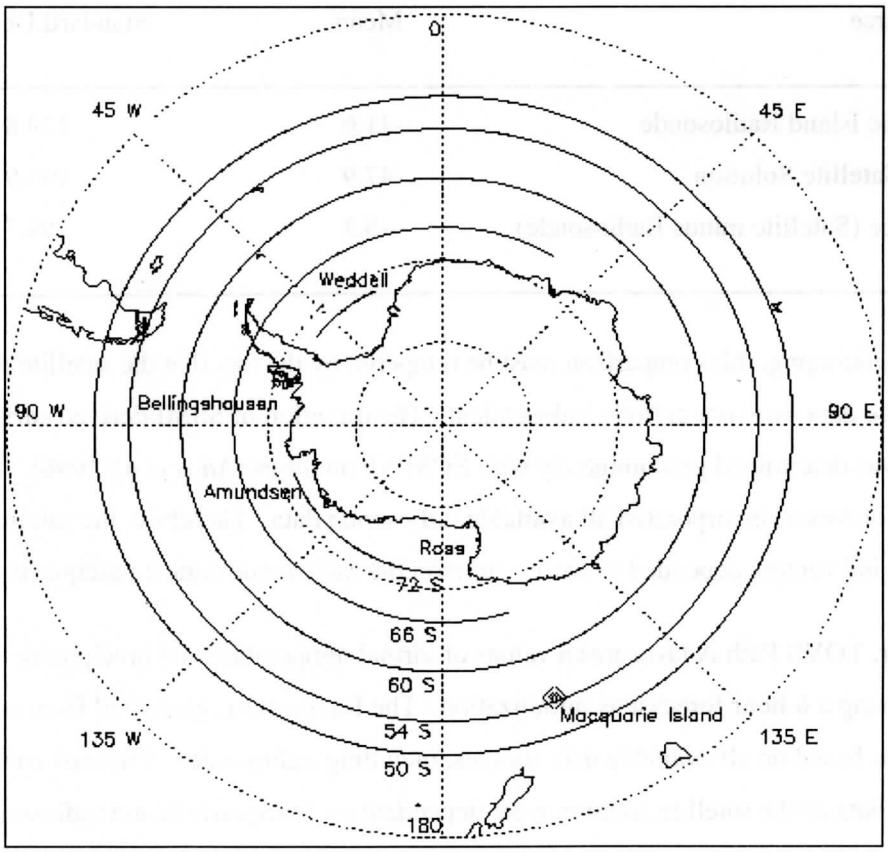

4. MOISTURE TRANSPORT ACROSS THE SOUTHERN OCEAN

4.1 Zonal averages

Using the methodology outlined previously, vertically integrated meridional moisture transports were generated for 1988 across the latitudinal boundaries shown in Figure 2. Zonal averages were computed and are shown in Figure 3 along with values from several previous studies. Across 50°S, the satellite-measured meridional moisture flux is -31.8 kg m^{-1} s^{-1}, approximately 25% larger than the next largest flux value. There is no sea ice and almost no land mass at this latitude. The satellite solution is optimized with plentiful SSM/I surface wind speed data. Because traditional analyses suffer from data scarcity here, the satellite measurements offer a superior moisture flux answer in this region of the world. Although only data from 1988 were used for the satellite solution, interannual variability cannot account for the given discrepancy over such a large planetary region. The satellite-measured meridional moisture flux across 60°S of -15.2 kg m^{-1} s^{-1} is closer to a median or consensus value. Contemporary research by *Bromwich et al.* (1995) and *Giovinetto et al.* (1997) indicates -17.0 kg m^{-1} s^{-1} and -17.8 kg m^{-1} s^{-1} respectively for meridional moisture flux here.

4.2 Longitudinal dependence of moisture transport

The 1988 meridional moisture transport across 50°S encompasses large longitudinal variability as shown in Figure 4. Poleward moisture flux reaches a maximum of 60 kg m^{-1} s^{-1} near 135°E midway between Australia and Antarctica. Values drop near the dateline before increasing to 45 kg m^{-1} s^{-1} at 120°W in the southeastern Pacific. Moisture flux is actually equatorward east of South America. Poleward moisture transport returns in the south central Atlantic.

Longitudinal dependence of moisture flux across 60°S is also shown in Figure 4. Maximum poleward moisture transport of 20-30 kg m^{-1} s^{-1} occurs from the southeastern Indian through the southern Pacific Oceans. Moisture flux changes abruptly as a function of longitude through the Drake Passage, becoming equatorward from there into the southwestern Atlantic. The southeastern Atlantic exhibits a small poleward moisture transport of 5-10 kg m^{-1} s^{-1}. From 30°W through 35°E, poleward moisture flux gradually increases. This pattern repeats from 55°E to 120°E but the rate of increase is faster. These results are consistent with two quasi-stationary cyclones situated just off the Antarctic coast at the same locations determined by *Bromwich* (1988).

Figure 3. Zonally averaged, vertically integrated meridional moisture transport (kg m^{-1} s^{-1}) for the satellite data solution in comparison to several previous studies.

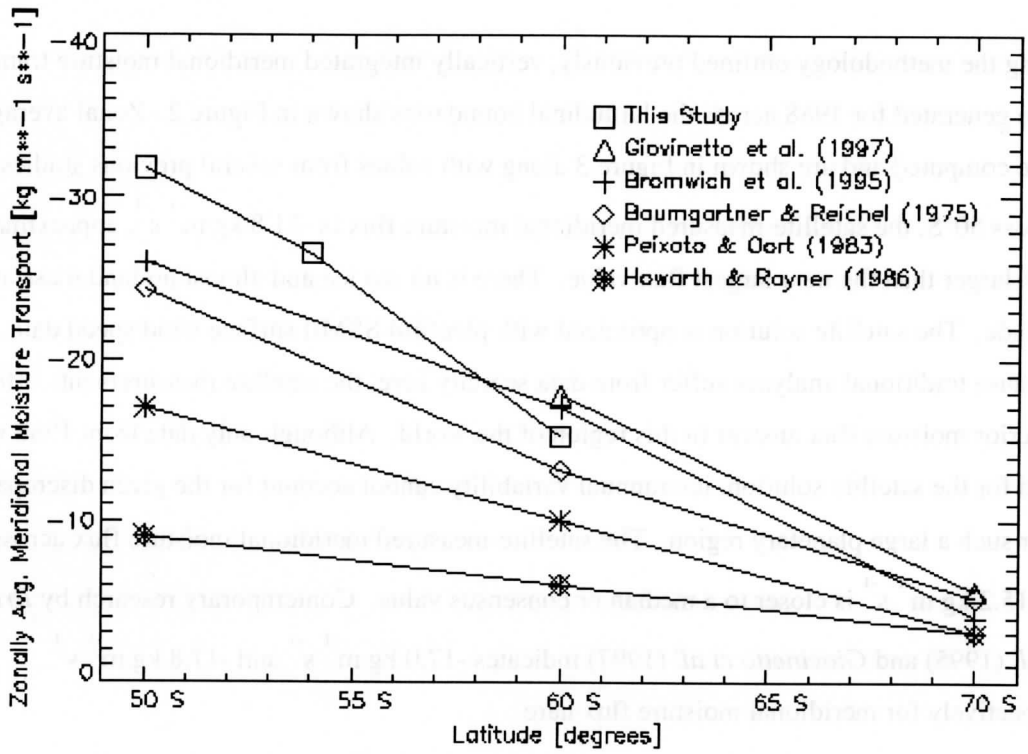

Figure 4. Vertically integrated meridional moisture transport (kg m^{-1} s^{-1}) across 50°S (left) and 60°S (right) plotted versus longitude. Plot has been smoothed with a five-point boxcar filter. Original data were overplotted for reference.

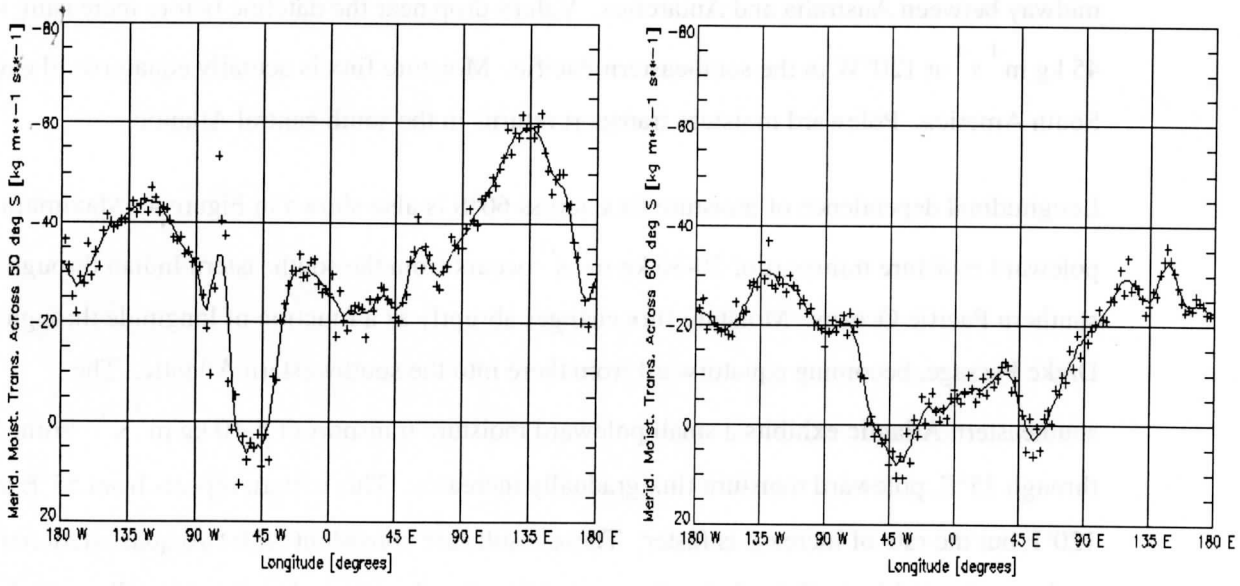

A critical assumption of this analysis is that the total vertical wind shear be approximately equal to the geostrophic wind shear. This assumption is not valid in the katabatic wind regime close to the continent where the boundary layer is decoupled from the atmosphere above. Therefore, only subsets of 66°S and 72°S could be analyzed for meridional moisture flux.

4.3 Vertical and sector dependence of moisture transport into West Antarctica

Figure 5 indicates the locations of the Ross Sea, Amundsen Sea, Bellingshausen Sea, and Weddell Sea sectors of West Antarctica. Meridional moisture fluxes across 66°S are presented in Figure 6 for vertical layers within each sector. This analysis illuminates atmospheric moisture sources for West Antarctic net precipitation. The largest poleward moisture transport occurs through the Amundsen Sea sector. The relative importance of the mid-troposphere increases at higher latitudes with respect to transporting moisture through the Amundsen Sea (not shown). Large poleward moisture transport is also evident through the Bellingshausen Sea. The relative importance of vertical layers does not change from 60°S to 66°S for the Bellingshausen Sea (not shown) in contrast to the results for the Amundsen Sea. Moisture transport through the Weddell Sea sector is primarily invariant, exhibiting equatorward flux at all levels. For net precipitation onto the Antarctic ice sheets, moisture transport through other sectors must compensate for an actual loss of atmospheric moisture across the Weddell Sea.

5. NET PRECIPITATION

Using the transport results from Figure 4, the moisture convergence for 50-60°S latitude band was determined to be 636 kg m^{-2} yr^{-1}. Only *Briazgin and Sharova* (1978) and *Strokina and Krhol* (1978) found a higher value for moisture convergence. All other studies indicated smaller convergence. This region is problematic for studies with conventional data due to a dearth of surface and upper-air observations. Analyses and methodologies employed by other studies required large-scale interpolation through this region of scarce in situ data.

The satellite solution is invalid along the Antarctic coastline because geostrophy cannot explain the vertical wind shear in these regions of persistent katabatic drainage. The smallest region was defined for which reasonable net precipitation estimates can be made using the outlined satellite data and methodology. The meridional moisture flux across 66°S was used wherever possible from ~161°E eastward around West Antarctica to ~31°E. The remainder of longitudes along most of the East Antarctic coastline used the meridional moisture flux values across 60°S. This region encloses an area of 26,375,300 km^2, which is a little less than twice the area of the actual

Figure 5. West Antarctica showing boundaries used in sector analyses. Solid lines indicate the longitude borders of defined sectors. Meridional moisture flux was analyzed across latitude boundaries shown with dashed lines.

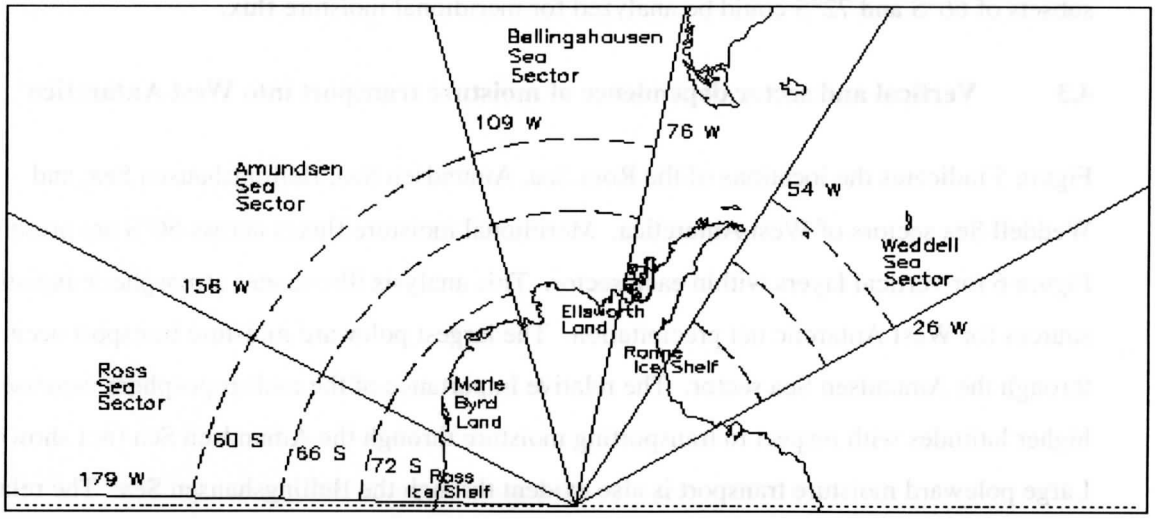

Figure 6. Comparison of vertically integrated meridional moisture transport (kg m^{-1} s^{-1}) across 66°S for individual vertical layers within the Ross Sea (lower left), Amundsen Sea (upper left), Bellingshausen Sea (upper right), and Weddell Sea (lower right) sectors. Negative values indicate poleward moisture flux.

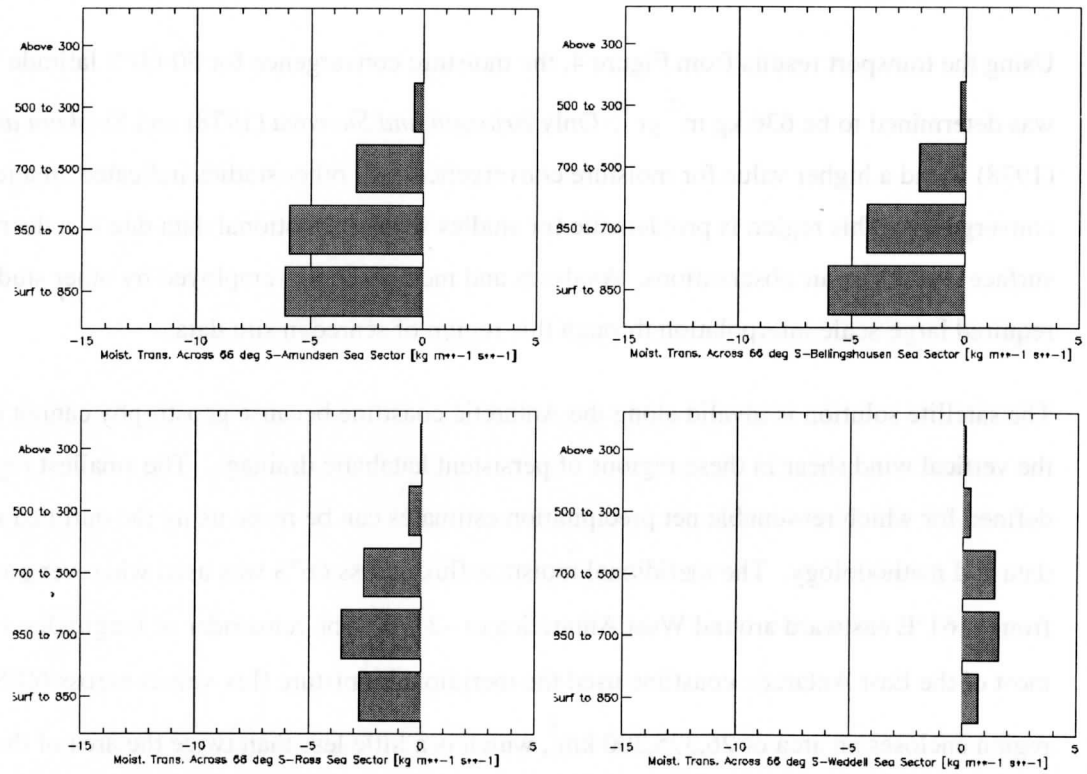

continent. The defined area includes the Antarctic continent, ice shelves, and a fraction of the surrounding seas. Atmospheric moisture convergence for this region implies a net precipitation of 21.8 cm yr^{-1}.

Although no direct measurement of net continental precipitation was possible, an indirect estimate could be extrapolated. The average gradients from other studies (*Baumgartner & Reichel* (1975), *Peixoto & Oort* (1983), *Howarth & Rayner* (1986), *Bromwich et al.* (1995), *Giovinetto et al.* (1997)) were used to extrapolate the satellite solution to the Antarctic coastline. Assuming that the zonal moisture flux through the longitudinal boundaries at 31°E and 161°E cancel, extrapolated moisture fluxes indicate net Antarctic precipitation of 17.4 cm yr^{-1}.

6. CONCLUSIONS

The strength of the satellite-derived solution is its spatial and temporal data coverage over the ice-free Southern Ocean. Data from 1988 were analyzed. Comparisons between the Macquarie Island radiosonde and the satellite-derived moisture flux estimates indicated small bias, however the satellite-derived products were not entirely independent of the radiosonde data.

Zonally averaged meridional moisture flux across 50°S of -31.8 kg m^{-1} s^{-1} is higher than indicated by contemporary studies, while the flux across 60°S of -15.2 kg m^{-1} s^{-1} is closer to a consensus value. Resulting moisture convergence for the 50-60°S latitude band is 636 ± 50 kg m^{-2} yr^{-1}, about 50% larger than reported by *Baumgartner and Reichel* (1975) and *Bromwich et al.* (1995).

From 50°S to 60°S, longitudinal patterns of meridional moisture flux are consistent between latitudes. Poleward transport peaks in the South Pacific near 135°E with a secondary maximum close to 135°W. The moisture flux changes abruptly as a function of longitude through the Drake Passage. Moisture transport actually becomes equatorward in the Weddell Sea.

Moisture convergence poleward of 60°S yielded a net precipitation of 28.1 cm yr^{-1} comparing favorably with 31.4 cm yr^{-1} and 32.9 cm yr^{-1} from *Bromwich et al.* (1995) and *Giovinetto et al.* (1997) respectively. Satellite analysis can be utilized for an enclosed area bounded meridionally by 60°S along East Antarctica and 66°S around West Antarctica. Satellite-derived moisture convergence for this region yielded a net precipitation of 21.8 cm yr^{-1}. By utilizing other studies, the satellite solution was extrapolated to the Antarctic coastline. Resulting net precipitation for Antarctica itself was determined as 17.4 ± 1.4 cm yr^{-1}.

Large moisture transport into West Antarctica occurs through the Amundsen and Bellingshausen Seas. Equatorward moisture flux is exhibited throughout the Weddell Sea. The Amundsen and Bellingshausen sector fluxes must supply all the moisture for West Antarctic net precipitation in addition to deficits through the Ross and Weddell sectors. These atmospheric moisture flow patterns suggest enhanced net precipitation over Ellsworth and Marie Byrd Land and corresponding reduced net precipitation over the Ross and Ronne Ice Shelves. Moisture flux across the Amundsen Sea is more apt to reach interior regions of the West Antarctic Ice Sheet because much of the transport is accomplished through the mid-troposphere. Moisture flux across the Bellingshausen Sea, which is preferentially advected in the lowest layers, is largely precipitated on the Ellsworth Coast.

7. ACKNOWLEDGMENTS

Joel Susskind and Paul Piraino provided the TOVS Path A data. Robert Atlas and Joe Ardizzone supplied the SSM/I-derived surface vector wind fields. Richard Cullather provided the Macquarie Island radiosonde data. David Bromwich and Richard Cullather added many thoughtful comments during the development of this project. This study was supported by NASA grant W18,795 to the second author.

8. REFERENCES

Atlas, R., R. N. Hoffman, and S. C. Bloom, 1993. Surface wind velocity over the oceans. In Atlas of Satellite Observations Related to Global Change, edited by R. J. Gurney, J. L. Foster, and C. L. Parkinson, 129-139, Cambridge University Press, Cambridge, Great Britain.

Atlas, R., R. N. Hoffman, S. C. Bloom, J. C. Jusem, and J. Ardizzone, 1996. A multiyear global surface wind velocity dataset using SSM/I wind observations. Bull. Am. Meteorol. Soc., 77, 869-882.

Baumgartner, A., and E. Reichel, 1975. The World Water Balance. 179 pp., Elsevier, Amsterdam, The Netherlands.

Briazgin, N. N., and V. J. Sharova, 1978. Fresh-water balance of the world ocean-precipitation. In World Water Balance and Water Resources of the Earth, edited by V. I. Korzun, A. A. Sokolov, M. I. Budyko, K. P. Voskresensky, G. P. Kalinin, A. A. Konoplyantsev, E. S. Korotkevich, P. S. Kuzin, and M. I. Lvovich, 548-561, UNESCO press, Leningrad, USSR.

Bromwich, D. H., 1988. Snowfall in high southern latitudes. Rev. Geophys., 26, 149-168.

Bromwich, D. H., F. M. Robasky, R. I. Cullather, and M. L. Van Woert, 1995. The atmospheric hydrologic cycle over the Southern Ocean and Antarctica from operational numerical analyses. Mon. Weather Rev., 123, 3518-3538.

Douglas, B. C., 1991. Global sea level rise. J. Geophys. Res., 96, 6981-6992.

Giovinetto, M. B., K. Yamazaki, G. Wendler, and D. H. Bromwich, 1997. Atmospheric net transport of water vapor and latent heat across 60°S. J. Geophys. Res., 102, 11,171-11,179.

Goodberlet, M. A., C. T. Swift, and J. C. Wilkerson, 1990. Ocean surface wind speed measurements of the Special Sensor Microwave/Imager (SSM/I). IEEE Trans. Geosci. Remote Sensing, 28, 823-828.

Hollinger, J., R. Lo, G. Poe, R. Savage, and J. Peirce, 1987. Special Sensor Microwave/Imager User's Guide. 120 pp. (Available from Naval Research Laboratory, Code 7223, 4555 Overlook Ave., S.W., Washington, DC 20375, USA)

Howarth, D. A., and J. N. Rayner, 1986. Estimates of sources and sinks of atmospheric moisture in the Southern Hemisphere. In Proc. Second Intl. Conf. on Southern Hemisphere Meteorology, 163-166, Am. Meteorol. Soc., Wellington, New Zealand.

Kreyszig, E., 1962. Advanced Engineering Mathematics. 939 pp., John Wiley and Sons, New York, USA.

Lorius, C., 1983. Accumulation rate measurements on cold polar glaciers. In The Climatic Record in Polar Ice Sheets, edited by G. de Q. Robin, 65-70, Cambridge University Press, Cambridge, Great Britain.

Peixoto, J. P., and A. H. Oort, 1983. The atmospheric branch of the hydrological cycle and climate. In Variations in the Global Water Budget, edited by A. Street-Perrott, M. Beran, and R. Ratcliffe, 5-65, D. Reidel, Boston, USA.

Slonaker, R. L., and M. L. Van Woert, 1999. Atmospheric moisture transport across the Southern Ocean via satellite observations. J. Geophys. Res., in press.

Strokina, L. A., and V. P. Krhol, 1978. Fresh-water balance of the world ocean-evaporation. In World Water Balance and Water Resources of the Earth, edited by V. I. Korzun, A. A. Sokolov, M. I. Budyko, K. P. Voskresensky, G. P. Kalinin, A. A. Konoplyantsev, E. S. Korotkevich, P. S. Kuzin, and M. I. Lvovich, 561-568, UNESCO press, Leningrad, USSR.

Susskind, J., and J. Pfaendtner, 1989. Impact of interactive physical retrievals on NWP. In Report on the Joint ECMWF/EUMETSAT Workshop on the Use of Satellite Data in Operational Weather Prediction: 1989-1993, 1, edited by T. Hollingsworth, 245-270.

Susskind, J., P. Piraino, L. Rokke, L. Iredell, and A. Mehta, 1997. Characteristics of the TOVS Pathfinder Path A dataset. Bull. Am. Meteorol. Soc., 78, 1449-1472.

Wallace, J. M., and P. V. Hobbs, 1977. Atmospheric Science. 467 pp., Academic Press, San Diego, USA.

TECHNICAL PROCEEDINGS OF THE TENTH INTERNATIONAL ATOVS STUDY CONFERENCE

Boulder, Colorado

27 January - 2 February 1999

Edited by

J. Le Marshall and J.D. Jasper

Bureau of Meteorology Research Centre, Melbourne, Australia

Published by

Bureau of Meteorology Research Centre

PO Box 1289K, GPO Melbourne, Vic., 3001, Australia

December 1999